Mesenchymal stem cells transplantation combined with IronQ attenuates ICH-induced inflammation response via Mincle/Syk signaling pathway

Guoqiang Yang
Southwest Medical University
Jiraporn Kantapan
Chiang Mai University Faculty of Associated Medical Sciences
Maryam Mazhar
Southwest Medical University
Xue Bai
Southwest Medical University
Yuanxia Zou
Southwest Medical University
Honglian Wang
Southwest Medical University
Bingfeng Huang
Southwest Medical University
Sijing Yang
Southwest Medical University
Nathupakorn Dechsupa
Chiang Mai University Faculty of Associated Medical Sciences
Li Wang (wangli120@swmu.edu.cn)
Southwest Medical University https://orcid.org/0000-0003-3881-3149

Research Article

Keywords: Mesenchymal stem cells, IronQ, Intracerebral hemorrhage, Mincle, inflammatory response

Posted Date: August 15th, 2022

DOI: https://doi.org/10.21203/rs.3.rs-1791468/v1

Version of Record: A version of this preprint was published at Stem Cell Research & Therapy on May 15th, 2023. See the published version at https://doi.org/10.1186/s13287-023-03369-6.

Abstract

Background

Cerebral edema, inflammation, and subsequent neurological defecit, are the common consequences of intracerebral hemorrhage (ICH). Mesenchymal stem cells (MSCs) transplantation had been used as a neuroprotective therapy in nervous system diseases because of its anti-inflammatory effect. However, the survival, viability, and efficacy of MSCs are limited due to the severe inflammatory response after ICH. Therefore, ways to improve the survival and viability of MSCs will provide a hopeful therapeutic efficacy for ICH. Notably, the metal-quercetin complex via coordination chemistry has been verified positively and studied extensively for biomedical applications, including growth-promoting and imaging probes. Previous studies have shown that the iron-quercetin complex (IronQ) has excellent dual functions with a stimulating agent of cell growth and an imaging probe for magnetic resonance imaging (MRI). Therefore, we hypothesized that IronQ could improve the survival and viability of MSCs, displaying the anti-inflammation function in the treatment of ICH, while also label MSCs for their tracking by MRI. This study was designed to investigate the effects of the combined treatment of MSCs with IronQ on inflammation and elucidate their underlying mechanisms.

Methods

A collagenase I-induced ICH mice model was extablished, which were randomly divided into model group (Model), quercetin gavage group (Quercetin), MSCs transplantation group (MSCs), and MSCs transplantation combined with IronQ group (MSCs + IronQ). Then the neurological deficits score, brain water content (BWC), and the protein expression levels of IL-6, TNF-α, NeuN, MBP, and GFAP were investigated. We measured the protein expression levels of Mincle and its downstream targets. Furthermore, the lipopolysaccharide (LPS)-induced BV2 cells was used to investigate the neuroprotection of conditioned medium of MSCs co-cultured IronQ in *vitro*.

Results

We found that the combined treatment improves the inflammation-induced neurological function and BWC by inhibiting the Mincle/Syk signaling pathway in *vivo*. The conditioned medium of MSCs co-cultured with IronQ decreased inflammation, the protein expression levels of Mincle, and its downstream targets in LPS-induced BV2 cell line.

Conclusions

These data suggested that the combined treatment plays a synergistic role in ameliorating the consequences of ICH, including neurologic deficits, brain edema, and inflammatory response through the

downregulation of the Mincle/syk signaling pathway.

1. Background

Intracerebral hemorrhage (ICH) is a common stroke syndrome, accounting for a disproportionate amount of stroke-induced neurological morbidity and mortality, which is estimated to have more than 5 million brain hemorrhage cases and nearly 2.8 million deaths worldwide each year (1–5). Although less common than ischemic stroke, ICH is the primary reason for stroke-induced mortality, and there is not yet a critical therapy beyond supportive care in clinical practice (6–9). After ICH, a large intracranial hematoma always leads to primary brain injury (PBI) through the destruction of brain tissue and the high intracranial pressure (10). Previous studies have revealed that craniotomy for hematoma evacuation and minimally invasive endoscopic procedures effectively limit PBI following ICH (11). However, early surgery shows no improvement in long-term outcomes compared with initial conservative treatment (12). Increasing evidence shows that red blood cell debris, hemoglobin, and its degradation products such as Iron and blood components trigger secondary brain injury (SBI) following ICH and contribute to a series of damaging events, including neuroinflammation, brain edema, oxidative stress, blood-brain barrier damage, demyelination, axonal damage, and neuronal death (3, 13–17). More than 30% of the ICH survivors live with severe movement dysfunction, and over 70% of these patients suffer cognitive impairment (18, 19). Recently, an increasing number of studies have been conducted to focus on the ICH-induced SBI to investigate promising therapeutic targets after ICH.

Mesenchymal stem cells (MSCs) are considered the promising seed cells for nervous system diseases because they have weak immunogenicity, good safety, and ease of cultivation (20–22). It has been confirmed that MSCs can improve neurological functional recovery following ICH (8). However, the transplanted MSCs display limited ability to repair the damaged tissue because of their poor survival rate in brain disease (23). Numerous studies have shown that single herbs and herb extracts in traditional Chinese medicine (TCM) have specific roles in regulating the proliferation and differentiation of MSCs. Quercetin, a flavonoid widely distributed in various herbs, fruits, and vegetables, has been proved to improve neuronal function in repairing brain injury, probably by inhibiting inflammatory response and apoptosis (24). Quercetin can regulate cell proliferation, migration, autophagy, and other biological functions, thus exerting antioxidant and anti-inflammatory effects (23, 24). However, quercetin's poor water solubility, chemical instability, and low bioavailability significantly limit its biomedical applications. Nathupakorn et al. have synthesized the Iron-quercetin complex (IronQ), which has excellent dual functions using an imaging probe for magnetic resonance imaging (MRI) and a stimulating agent of peripheral blood mononuclear cells (PBMCs) growth (25, 26). If IronQ could be used to improve MSCs growth to enhance the therapeutic effects after ICH, it would be a promising therapy for relieving brain injury.

The immune system plays an essential role in the inflammatory response. Compared with the adaptive immune system (which is highly pathogen-specific), innate immune receptors recognize a variety of pathogens with similar structures (27–29). As an essential innate immune cell of the central nervous

system, microglia are usually regarded as the macrophages of brain tissue. A growing piece of evidence suggests that the inflammatory response plays a vital role in brain damage after ICH. Meanwhile, inflammatory factors released by activated microglia can aggravate the inflammatory damage to brain tissue, while chemoattractant peripheral inflammatory cells infiltrate the central nervous system (CNS), which aggravates the inflammatory response of the CNS (7). Microglia is the primary source of Interleukin-6 (IL-6) and Tumour necrosis factor α (TNF-α) after ICH. Macrophage-inducible c-type lectin (Mincle) is a newly discovered non-typical c-type lectin receptor (innate immune receptor), which is mainly expressed in microglia/macrophages (30). Stimulated by certain fungi, mycobacterium tuberculosis, and necrotic cells, it binds to the associated ligand (SAP130), phosphorylating downstream syk and activating card9-dependent cascade signals (30, 31). The content of Card 9 is directly related to the effect of the immune response, and the card9-bcl10-malt1 complex plays a crucial role in activating the nuclear factor-kappa B (NF-κB) pathway (32, 33). Activation of the NFκB pathway leads to the expression of inflammatory factors that play a role in the host's innate immune response, suggesting that Mincle is a crucial target for regulating microglia/macrophage cell polarization. The Mincle/Syk pathway plays a role in traumatic brain injury (30), subarachnoid hemorrhage, and ischemic stroke (31–33). However, the regulatory mechanism of the Mincle/Syk pathway in ICH remains unclear.

In this experiment, we examined the effects of combined treatment of MSCs with IronQ on the neurological deficits score, brain water content (BWC), protein expressions levels of neuron-specific nuclear (NeuN, a marker of neurons), myelin basic protein (MBP, a marker of myelin), glial fibrillary acidic protein (GFAP, a marker of astrocytes), as well as the inflammatory factors in mice with ICH and Mincle, and its downstream were also investigated to explore the neuroprotective effect, anti-inflammatory function and the underlying mechanisms of combined treatment.

2. Materials And Methods

2.1 Chemicals

The IronQ complex was synthesized according our previous study (25). Briefly, 0.0050 mole of Quercetin hydrate (Sigma, USA) was added to 500 mL HPLC-methanol (Sigma, USA) in round bottles with continued stir until complete dissolution of quercetin hydrate and the color of the solution turns yellow. The quercetin hydrate solution was then slowly adjusted to a pH of 12 by the addition of 50% (w/v) NaOH solution to ovtain a deprotonated form of quercetin. 0.0025 mole Iron (III) chloride (Sigma, USA) in 500 mL ultrapure water (up water) was freshly prepared and then blended with the deprotonated quercetin solution until the color of the combined solution changed to dark yellow, which was followed with incubation at 60°C for 2 h under continuous stirring. And then the combined solution was purified by the dialysis method and then evaporated to dryness. Collected the dark powder product, stored it in a desiccator at room temperature (RT) and kept away from the light.

2.2. Animals

Sixty male wild-type C57BL/6 mice at the age of 8–9 weeks, weighed between 22 and 25g, were purchased from Chongqing Tengxin Biotechnology Co., Ltd (Chongqing, China). All of them were housed in the same animal care facility, such as standard temperature (23 ± 2°C), lighting (12/12-h light/dark cycle), relative humidity (65 ± 5%), and free access to food and water. The procedure for using the animals followed the Guidance Suggestions for the Care and Use of Laboratory Animals formulated by the Ministry of Science and Technology of China. The animal protocol was approved (Approval No. 20211122-040) by the Animal Ethical Committee of the Animal Center of Southwest Medical University (Luzhou, Sichuan), and the experimental procedures were optimized to minimize the number of animals and alleviate the pain felt by the experimental animals. The mice were randomly divided into six groups: the sham group (Sham), the model group (Model), quercetin gavage group (Quercetin), MSCs transplantation group (MSCs), MSCs transplantation combined with IronQ group (MSCs + IronQ), and MSCs + IronQ control group, which were assigned to the following five experimental procedures, respectively (Fig. 1A).

2.3. Intracerebral Hemorrhage Mice Model

Mice anesthetized intraperitoneally at a dose of 40 mg/kg of 1% pentobarbital sodium were fixed on a stereotaxic apparatus (in a prone position) and kept the anterior and posterior fontanels at the same level. The scalp was incised sagittally about 1cm, exposing the anterior fontanelle with 30% H_2O_2. The mixture containing 1μL 0.15 U/μL collagenase I (C8140, Solarbio, China) and supplementary 0.9% normal saline was extracted with a 1μL microsyringe. A burr hole (1 mm) was drilled on the right calvaria bone at the point, which was 2.5 mm lateral and 0.2 mm anterior to the anterior fontanelle. The needle was fixed on the stereotaxic apparatus and inserted into the caudate nucleus (location: 3 mm depth to the hole), and the mixture was slowly injected (Fig. 1B). After injection, the burr hole was sealed with bone wax, and the skin was sutured. The mice in the sham group performed the same procedure except that the mixture was not injected, and the mice in the MSCs + IronQ control group were given the injection of the complex of MSCs with IronQ. The mice in the quercetin group for intragastric administration with quercetin (50 mg/kg/day) after 24 hours when successfully modeled was conducted according to the previous study (23, 24). The conceptual illustrations of the experimental protocols are given in Fig. 1. After successfully modeled, the mice in the sham group, model group, and MSCs + IronQ group were imaged under 3.0T MRI.

2.4 Neurological Function Assessment by Modified neurologic severity score (mNSS) Test

The mNSS was operated as previous reported (34). Neurologic deficits were performed by evaluating abnormal movements, including motor, sensory, and reflex deficits at 24 h after ICH induction using the mNSS system (18-point neurological deficit scale), which is widely administrated to evaluate the degree of ICH-induced nerve injury. The higher score resprents the more severely neurological damage. After 24 h of the ICH model constructed by the right caudate nucleus injection of collagenase, mice were evaluated and scored blindly.

2.5. Extraction, Passage, and Identification of MSCs

The method for obtaining MSCs was described previously (35). Briefly, after intraperitoneal injection of 1% pentobarbital sodium until muscle relaxation, the femurs and tibias were isolated from the male healthy C57BL/6 mice on the condition of asepsis. Then, carefully remove the muscles on the bone with a scissor and sterile dust-free paper, and pay attention not to break the bone. After washing the bones with sterile PBS three times (1 minute for update) and then soaking in 70% alcohol for 30 s for surface sterilization, their medullary cavities were iteratively washed by Dulbecco's modified eagle medium (DMEM, Gibco, USA) sucked with a 5 mL syringe to acquire a uniform suspension with mixed cells. Centrifuge the cells at 1,500 rpm for 5 min, and red blood cells were removed by red blood cell lysate (R1010, Solarbio, China). Followed by suspending these cells, they were cultured with DMEM plus 10% fetal bovine serum (FBS, Gibco, USA) as well as 1% penicillin/streptomycin (C0222, Beyotime Biotechnology, China) at 37°C in a humidified atmosphere containing 5% CO_2. Cells were utilized for subsequent experiments from 3rd passage. The 3rd passage cells were collected and resuspended in phosphate-buffered saline (PBS, 100 μL), containing 1×10^6 single cells, which were incubated with the primary antibodies against CD90, CD29, and CD45 (Bioscience, USA) at 37°C for 30 minutes. The identification of cells was performed on flow cytometry (BD FACSCanto , BD Biosciences, USA).

2.6. IronQ Labeling of MSCs and Determination of Labeling Efficiency by Prussian Blue

MSCs (1×10^6 cells, 5 mL) were seeded in a 6-well plate with the DMEM (Gibco, USA) in the presence of 10% FBS (Gibco, USA) and 1% penicillin/streptomycin (C0222, Beyotime Biotechnology, China). After MSCs adherence, IronQ solution (1000 μg/mL, IronQ dissolved with sterile up water) was added to the six-well plate at concentrations of 0, 50, 100, 200, and 400 μg/mL, and the plate then continued to be incubated in a humidified incubator with 5% CO_2 at 37°C for 2 days. After the indicated time, the IronQ labeled cells, and other adherent cells were washed three times with PBS to remove any unbounded IronQ from the cells. To verify the intracellular IronQ uptake of MSCs, Prussian blue dye was used to stain the iron component. Next, the cells were fixed with 4% paraformaldehyde at 37°C in a humidified incubator for 20 min. After that, a fixative reagent was removed, and Perl blue reaction solution was added at a final volume of 1 mL for each well (G1422, Solarbio, China). The cells were then reincubated at 37°C for 30 min. After the indicated time, the cell morphology and positively blue-stained cells were observed under an inverted microscope (Nikon, Japan) and imaged.

2.7. Transplantation of MSCs and MSCs Combined with IronQ

MSCs and the combined of MSCs with IronQ at passages 3–6 were used for subsequent experiments. The cells were collected, and cell concentration was adjusted to 5×10^7 cells per mL. Then cells suspension (20 μL) was collected with a microsyringe and injected into the point (location: the right of anterior fontanelle: 3 mm; anterior of anterior fontanelle: 0.2 mm; depth: 3 mm) of mouse brains for

MSCs, MSCs + IronQ, and MSCs + IronQ control groups respectively at an injection rate of 2 μL/min after 24 hours when the mice were successfully modeled. Then the needle hole was sealed with bone wax, and the skin was sutured and disinfected.

2.8. Magnetic Resonance Imaging of MSC^{IronQ} transplant in ICH Mice

Mice were anesthetized with at a dose of 40 mg/kg of 1% pentobarbital sodium throughout MRI examination. MRI was performed by a 3-Tesla (Siemens, Germany) at the Affiliated Traditional Chinese Medicine Hospital of Southwest Medical University. It was used a T1 fast spin-echo (repetition time/echo time = 500/11 ms) with a field of view of 16 × 16 mm^2, matrix of 256 × 256 and 0.75-mm thick for coronal, axial, and sagittal plane. The single image was preserved as 1019 × 602 pixel picture for T1 lesion evaluation.

2.9. Hematoxylin and Eosin and Nissl Staining

As described earlier, the perfusion-fixed brain tissues were further underwent immersion fixation in 4% formaldehyde overnight (36). Then, the tissues were dehydrated in a series of graded alcohols and then in xylene for 30 min each. Later, the brain tissues were embedded via paraffin and were cut into pieces of 4 μm thickness at the coronal plane using a microtome (RM 2245, Leica, Germany). For staining, the tissue slides were dewaxed and rehydrated. Hematoxylin and Eosin (HE) staining was carried out according to the standard procedure. Similarly, Nissl staining was performed according to the manufacturer's instructions. The slides were observed under a microscope (DM500, Leica, Japan), and images were captured using software Leica application suite X, at a magnification of 200 x.

2.10. Brain Water Content Examination

Brain water content was measured as previously reported (37). Briefly, animals were anesthetized and then decapitated. The brain samples were quickly removed and weighed immediately on a precise electronic balance to determine the wet weight. After dried in the thermostat for 24 h at 100 °C, the brain samples were weighed again to measure dry weight. Brain water content is calculated as [(wet weight – dry weight)/wet weight] × 100%.

2.11. Immunofluorescence Staining

Immunofluorescence staining was performed as previously reported (37). Under deep anesthesia, the mice were transcardially perfused with 0.9% normal saline and 4% paraformaldehyde in 0.01 M phosphate buffer saline (PBS, pH7.4) successively. Then the brain samples were harvested, post-fixed in 4% paraformaldehyde at 4°C for 24 h, and dehydrated for an additional 1 day in the 30% sucrose solution until the samples sank to the bottom of the sucrose solution. The samples in optimal cutting temperature compound (OCT) were cut coronally for 4-μm sections at the level of basal ganglion by using the freezing microtome (CM1950, Leica, Germany). After washing with PBS three times, tissues on glass slides were

blocked with 5% BSA for 1 h at RT and then incubated with primary antibodies, including mouse anti-IL-6 (sc32296, Santa Cruz, USA, diluted 1:100), mouse anti-TNF-α (sc52746, Santa Cruz, USA, diluted 1:100), mouse anti-Mincle (sc390806, Santa Cruz, USA, diluted 1:100), rat anti-F4/80 (sc52664, Santa Cruz, USA, diluted 1:100), rabbit anti-GFAP (16825-1-AP, Proteintch, USA, diluted 1:100), rabbit anti-MBP (10458-1-AP, Proteintech, USA, diluted 1:100), and rabbit anti-NeuN (12943, CST, USA, diluted 1:100) overnight at 4°C. The next day, tissues were washed with PBS three times 5min each, followed by incubation with Alexa Fluor® 555 conjugated anti-mouse secondary antibody (A21424, Life Technologies, USA, diluted 1:500), Alexa Fluor™ 488 conjugated anti-mouse secondary antibody (A11001, Invitrogen, USA, diluted 1:500), and Alexa Fluor™ 488 conjugated anti-rabbit secondary antibody (A11034, Invitrogen, USA, diluted 1:500) at RT for 1 hour. The images were captured by Fluorescence orthotopic microscope (DM4B, Leica, Germany).

2.12. Western Blot

Under deep anesthesia, the mice were decapitated, and brain samples were quickly harvested and separated into ipsilateral brain hemispheres, which were homogenized in RIPA lysis buffer (Beyotime, China) for protein extraction, and supernatants were collected after centrifugation at 4°C for 30 min at 13,000 rpm. Then the concentration of total protein for every sample in different groups was quantified by bicinchoninic acid (BCA) protein assay (Beyotime, China). Equal amounts of protein samples (50 μg) loaded with sodium dodecyl sulfate polyacrylamide gel electrophoresis (SDS-PAGE) were blotted to polyvinylidene fluoride (PVDF) membranes. Then, the membranes were incubated with the following primary antibodies against IL-6 (sc32296, Santa Cruz, USA, diluted 1:1000), TNF-α (sc52746, Santa Cruz, USA, diluted 1:1000), NeuN (12943, CST, USA, diluted 1:1000), MBP (10458-1-AP, Proteintech, USA, diluted 1:1000), Mincle (sc390806, Santa Cruz, USA, diluted 1:1000), syk (13198, CST, USA, diluted 1:1000) and p-syk (2710, CST, USA, diluted 1:1000), NFκB-p65 (sc8008, Santa Cruz, USA, diluted 1:1000), p-NFκB-p65) (3033, CST, USA, diluted 1:1000), and GAPDH (Abcam, diluted 1:10000) at 4°C overnight. After incubated with Alexa Fluor™ 790 conjugated anti-mouse secondary antibody (A11359, Invitrogen, USA, diluted 1:3000), Alexa Fluor™ 680 conjugated anti-mouse secondary antibody (A21109, Invitrogen, USA, diluted 1:3000), and Alexa Fluor™ 680 conjugated anti-rat secondary antibody (A21096, Invitrogen, USA, 1:3000) at RT for 2 h, the blots were exposed under a Far Infrared Laser Imaging System (Amersham Typhoon, USA). The protein levels were analyzed according to the corresponding amount of GAPDH by Image J software.

2.13. Real-Time Polymerase Chain Reaction Analysis

Total RNA was extracted from mouse brain tissue by using TRIzol reagent (11596026, Invitrogen, USA) following the manufacturer's protocol. One microgram RNA of each sample was reverse-transcribed into complementary DNA with HiScript III RT SuperMix for qPCR (+ gDNA wiper) (No.R323-01, Vazyme, China). The reaction was performed by using a fluorescent dye ChamQ Universal SYBR qPCR Master Mix

(No.Q711-02/03, Vazyme, China) in Mastercycler ep Realplex2 real-time PCR system (Eppendorf, Germany). Specific primers used in real-time PCR were purchased from Sangon Biotech (Shanghai) Co., Ltd and listed in Table 1.

Table 1
List of primers sequence

Gene Name	Primer sequence (5'-3')	Product Length
IL-6	F: AAAGAGTTGTGCAATGGCAATTCT	24
	R: AAGTGCATCATCGTTGTTCATACA	24
TNF-α	F: CATCTTCTCAAAATTCGAGTGACAA	25
	R: TGGGAGTAGACAAGGTACAACCC	23
Mincle	F: ACCAAATCGCCTGCATCC	18
	R: CACTTGGGAGTTTTTGAAGCATC	23
IL1β	F: TGCCACCTTTTGACAGTGATG	21
	R: AAGGTCCACGGGAAAGACAC	20
GAPDH	F: CGGAGTCAACGGATTTGGTCGTAT	24
	R: AGCCTTCTCCATGGTGGTGAAGAC	24

2.14. BV cell culture and experiments

Murine BV2 microglial cells were purchased from China Infrastructure of Cell Line Resource (Beijing, China) and cultured in high glucose DMEM (Gibco, Invitrogen) supplemented with 10% FBS (Gibco, Invitrogen), and 1% penicillin/streptomycin (C0222, Beyotime Biotechnology, China) at 37°C in a humidified incubator chamber under an atmosphere of 5% CO_2. The cells were incubated with LPS (200 ng/mL) and treated with the quercetin (Q), the conditioned medium of MSCs (M), the conditioned medium of MSCs + IronQ (M + Q) for 6 h and 24 h to check mRNA expression levels and protein expression levels respectively. Then the trehalose-6,6-dibehenate (TDB) (66758-35-8, invivogen, USA), a Mincle agonist, was used to active the mRNA and protein expression of Mincle. According the manufacturer' illustration, TDB was dissorved and made the concertration at 1mg/ml (DMSO/PBS:1/9) for store. BV2 cells were incubated with LPS (200ng/mL) and TBD (70μg/mL) in the absence of M + Q for 6 h and 24 h. Then BV2 cells were collected for the following qPCR and western blot expriments.

2.15. Statistical analysis

Parametric data were analyzed by GraphPad Prism 8 software and displayed as the mean ± standard error of the mean (SEM). Statistical differences between multiple groups were analyzed by one-way analysis of variance (ANOVA), and $P < 0.05$ was considered statistically significance.

3. Results

3.1. The Efficient MSCs Labeling and IronQ-labeled MSCs Tracking in the ICH Model Using T1-Weighted MRI

After the bone marrow was extracted from the tibia and femur of mice, the cells were cultured to the third passage and identified by their positive marker CD29 and CD90 and the negative marker CD45 (Fig. 2C). MSCs at passage 3–6 showed cluster growth (Fig. 2A). After incubated MSCs with IronQ (200 μg/mL) for 24 h, at 37 °C in a humified CO_2-incubator the labeling efficiency of IronQ for MSCs was identified by Prussian blue staining, and the labeled cells displayed blue colour (Fig. 2C). Figure 2E showed the T1-Weighted MRI images of mice brain in sham, Model, and MSCs + IronQ groups. The results displayed that the apparent hemorrhage (dark area) in the right caudate nucleus of mice in the model group can be observed in three MRI planes, including the coronal plane, axial plane, and sagital plane, compared with the mice in the sham group. After transplantation of MSCs + IronQ, MSCs labeled with IronQ were observed as a white spot present in the hemorrhage region under MRI.

3.2. MSCs and IronQ Combined Treatment Attenuated the Neurological Deficits and Protect the Brain Parenchyma and Neurons Survival after ICH

After 24 hours of the collagenase-induced ICH model, the mNSS system (18 points) was used for the assessment of neurological deficits for mice with ICH. Figure 3A displayed that the collagenase-induced ICH mice model has a similar level neurological deficits level ($P > 0.05$) compared with the mice in the Sham and MSCs + IronQ control groups ($P < 0.05$). After giving the three treatments to the ICH mice in these groups, the neurological deficits score in the three treatment (Quercetin, MSCs, and MSCs + IronQ) groups has remarkable improvement compared with the mice in ICH model group. The combined treatment improved the neurological deficits more significantly than the mice in quercetin and MSCs groups ($P < 0.05$). Meanwhile, the consistent results were also confirmed in the measurement of brain water content (Fig. 3B). Specifically, after 24 hours of the ICH model, the BWC was enhanced significantly compared with the mice in the sham group and MSCs + IronQ control groups ($P < 0.05$). Three treatments can decrease the BWC compared with the ICH model group. However, MSCs and the IronQ-labeled MSCs transplantation can attenuate the BWC more significantly compared with the quercetin gavage, and there is no significance between MSCs and MSCs + IornQ groups. Simultaneously, Fig. 3C displayed HE staining of brain tissue of mice in different groups, which revealed that the brain sections of mice from the sham group had no pathological changes, where neuropil was intact with normal texture; and healthy, nucleated pyramidal neurons were clearly observed. In the model group, obvious pathologic changes were observed in the perihematomal region of the brain. The neuropil was found to be less intact as compared to Sham brain tissue with signs of vacuolation, parenchymal loss, granulovacuolar neuronal

degeneration, neuronal shrinkage, reactive gliosis including relatively excessive number of oligodendrocytes, astrocytes, and microglia. MSCs + IronQ treatment maintained the normal neuropil architecture with less neuronal degeneration and less reactive gliosis observed compared with quercetin and MSCs therapy.

Nissl staining was also used to identify the ICH-induced neuronal injury since the loss of Nissl substance indicates the damage to neurons (Fig. 3D). It showed the presence of several blue-coloured nissl bodies in pyramidal neurons in normal brain. The nissl bodies display obvious pyknosis and swallow section phenomenon, that was further reduced in three treatment groups. MSCs + IronQ treatment revealed an increased number of nissl-stained neurons compared to quercetin and MSCs treatment groups, indicating its neuroprotective effect.

3.3. MSCs and IronQ Combined Treatment Enhanced the Expression Levels of NeuN, MBP, and GFAP in Mice with ICH

Figure 4 displayed immunofluorescence and western blot results for the protein expression levels of NeuN, MBP, and GFAP in different groups. Specifically, Fig. 4A-C showed that the uniformly distributed NeuN and MBP staining was observed throughout the brain tissue in the sham group, and after ICH, the expression levels of NeuN and MBP were decreased compared to the sham group, whereas the positive staining cells of NeuN and MBP increased in the treatment groups (Fig. 4A-B). The western blot results verified consistent results with the immunofluorescence, displaying that the protein expression level of GFAP in the sham group had a higher level than in the model group. However, after exerting the three treatments in mice with ICH, the protein expression levels of NeuN, MBP, and GFAP increased significantly compared with the mice in the model group. Moreover, no significance can be seen in the protein expression levels of NeuN and MBP in the three treatment groups, and only the GFAP' expression level in the MSCs + IronQ group was higher than in the quercetin ($P < 0.001$) and MSCs ($P < 0.05$) groups.

3.4. MSCs and IronQ Combined Treatment Decreased the Inflammatory Response in Mice with ICH

Figure 5A-D showed the double immunofluorescence of F4/80 (the marker of microglia), IL-6 and TNF-α. In the sham group, the F4/80 co-expression with IL-6 and TNF-α staining was not detectable. However, the uniformly distributed F4/80 co-expression with IL-6 and TNF-α staining was observed throughout the brain tissue. Interestingly, we found that positive expression of microglial IL-6 and TNF-α was associated with very weak staining in three treatment (Quercetin, MSCs, and MSCs + IronQ) groups. Moreover, the co-expression of F4/80 and IL-6, TNF-α could be seen as less positive-staining cells in MSCs + IronQ than in the other two treatment groups compared with the model group. Figure 5E-G displayed the results of western blot for the inflammatory factors, including IL-6 and TNF-α. The results showed that the protein expression level of IL-6 and TNF-α increased after ICH more significantly compared with the sham group ($P < 0.0001$). MSCs transplantation downregulated their expression levels more significantly than quercetin gavage ($P < 0.0001$), but the combined treatment decreased their expression levels remarkably compared with MSCs treatment ($P < 0.05$).

3.5. MSCs and IronQ Combined Treatment Regulated the Mincle/Syk Signaling Pathway for the Improvement of ICH Outcomes

Figure 6 showed the double immunofluorescence of Mincle and F4/80 and western blot of Mincle and its downstream in mice with ICH in different groups. The co-expression of Mincle and F4/80 was detected via double immunofluorescence (Fig. 6A). In sham brain sections, fewer positive co-expression cells of Mincle, and F4/80 were detected and their co-expression cells increased in mice with ICH. Conversely, after the combined treatment of MSCs and IronQ, the co-expression of positive cells level of Mincle and F4/80 was downregulated compared with the other two treatment groups, in which their co-expression was similar level (Fig. 6A).

Moreover, we further examined the protein expression levels of Mincle as well as its downstream (p-syk and p-NFκB-p65) via western blot. The immunoblotting results displayed that the protein expression levels of Mincle, p-syk, and p-NFκB-p65 increased obviously in Model group, and three treatments (Quercetin, MSCs, and MSCs + IronQ) downregulated their expression levels ($P < 0.0001$). MSCs transplantation decreased the expression levels of Mincle ($P < 0.05$) and p-NFκB-p65 ($P < 0.0001$) remarkably compared with quercetin gavage treatment, and no significance for p-syk can be seen between the MSCs and Quercetin. Positively, the combined treatment exerted the downregulation effects of the expression levels of Mincle and its downstream significantly compared with the other two treatment groups ($P < 0.05$) (Fig. 6B-E).

3.6. Conditioned Medium of The IronQ-labeled MSCs Reduce the mRNA and Protein Expression Levels of Mincle and Inflammatory factors in LPS-induced BV2 cells

Figure 7 showed the results of qPCR for Mincle and its related inflammation factors and western blot for the protein expression levels of Mincle and its related inflammation factors and p-syk in six cell groups, including BV2 control, BV2 + LPS, BV2 + LPS + Q, BV2 + LPS + M, BV2 + LPS+(M + Q), and its control. The mRNA expression levels of Mincle and its related inflammatory factors such as IL-6, TNF-α, and IL1β were assayed after 6 h of three treatments (Q, M, M + Q) for the LPS-induced BV2 cell line. The values of all the measured inflammatory factors and Mincle in inflammatory cell models increased significantly compared with the normal cell group but significantly reduced after giving the three treatments (Fig. 7A-D). Whereas there was no significance in mice with ICH between MSCs and Quercetin group, and the conditioned medium of MSCs with IronQ decreased the mRNA expression levels of Mincle, IL-6, and TNF-α more remarkably than MSCs' conditioned medium and quercetin intervention.

Moreover, we further investigated the protein expression levels of IL-6, TNF-α, Mincle, syk, and p-syk with western blot in 24h associated with the treatments of MSCs and MSCs with IronQ conditional medium and quercetin intervention in LPS-induced BV2 cell line. Figure 7E-I represents all the protein blotting results and analyses of this experiment. The protein expression levels of Mincle and p-syk displayed a significant escalating trend in the LPS-induced BV2 cell line compared with the normal group. All three treatments downregulated the protein expression levels of IL-6, TNF-α, Mincle, and p-syk ($P < 0.0001$). The

effect of the conditional medium of MSCs with IronQ decreased these protein expression levels more significantly than the conditional medium of MSCs compared with quercetin intervention.

3.7. Conditioned Medium of MSCs with IronQ Reduce the mRNA Levels of Mincle and its Related Inflammatory Factors and Exert the Therapeutic Effects by Regulating the Mincle/syk Signaling Pathway in LPS-induced BV2 cells

Figure 8 shows the results and analyses of qPCR for the mRNA expression levels of Mincle and its related inflammation factors and western blot for the protein expression levels of inflammation factors, Mincle, syk, p-syk, NFκB-p65, and p-NFκB-p65 in six cell groups. The mRNA expression levels of Mincle and its related inflammatory factors, including IL-6, and TNF-α were assayed after 6 h in the LPS-induced BV2 cell line. The values of all the measured inflammatory factors and Mincle in inflammatory cell models were significantly higher than that in the normal control group but significantly reduced by the conditional medium of MSCs with IronQ treatment (Fig. 8A-C). We further analyzed the protein expressions of IL-6, TNF-α, Mincle, syk, p-syk, NFκB-p65, and p-NFκB-p65 with western blotting after 24 h of LPS-induced BV2 cell line and MSCs + IronQ conditioned medium treatment. Figure 8D and 8G represent all the protein blotting results of this experiment. The Mincle and phosphorylated protein levels of syk and NFκB-p65 were significantly upregulated after the LPS-induced BV2 cell line. The conditional medium of MSCs + IronQ induced significant down-expression of Mincle, p-syk, and p-NFκB-p65 ($P < 0.0001$).

4. Discussion

Previously, many studies have verified that the molecular mechanisms of MSCs transplantation protect against brain damage displaying the therapeutic effects. Here, we utilized one complex named IronQ to combine (partly labeled) with the MSCs to inquire into the protective effects and underlying mechanisms on the ICH-injured brain. We found that the combined treatment of MSCs with IronQ attenuated the inflammation response to improve neurological deficits and brain edema in the perihematomal tissue of mice with ICH by inhibiting of the Mincle/Syk signaling pathway. The results suggested that MSCs combined with IronQ play a synergistic role in improving neurological function.

After ICH, perihematomal edema (PHE) occurs early, with a sharp increase of about 75% of its maximum volume during the first 24 hours, peak at three days showing an absolute growth, and lasts up to 14 days (8, 38–41). In humans, PHE is considered a radiological marker following ICH (42). Therefore, the extent of PHE both as a therapeutic target and a surrogate marker is associated with poor outcomes after ICH (39, 43). Thus, decreasing brain edema is critical for protecting against neurological deficits after ICH. In this study, our results displayed that the three treatments including quercetin, MSCs, and MSCs + IronQ, can alleviate the neurological deficits score and BWC in mice with ICH. The therapeutic efficacy of IronQ-labeled MSCs transplant and MSCs transplantation displayed a neuroprotective effect at the same level and significantly high efficacy than quercetin gavage treatment. In addition, the HE and Nissl staining also indicated the neuroprotection of IronQ-labeled MSCs is superior to MSCs and quercetin treatment, respectively. Preclinical studies have reported that quercetin improves behavioral recovery by

ameliorating inflammatory response after stroke (24, 44). It has been demonstrated that MSCs improve neurological outcomes and modulate the immune cells, including microglia, and neutrophils, to ameliorate inflammatory responses in rats after ICH (45, 46). Therefore, according to the above analyses, our results suggest that IronQ could upregulate the neuroprotective effect displaying the synergistic effect of decreasing PHE.

Previous studies have reported the axonal injury and demyelination in a collagenase-induced ICH rat model via immunofluorescent staining, and the authors found that obvious demyelination and axonal damage occurred inside and at the edge of the hematoma within 3 days in a collagenase-induced striatal ICH rat model, in which there was substantial neuron death (47). Moreover, Tao et al. have reported that the obvious demyelination and axonal damage on 3rd day in rats after primary brainstem hemorrhage (BSH) were extremely associated with brain edema and neurofunctional dysfunction resulting from hematoma (48). They found that on 3rd day after BSH, there was an evident reduction of MBP staining, which can be used for detection of intact axonal myelin in the brain region around the hematoma (48). It has been verified that reactive astrogliosis, which will be modulated to promote brain repair and reduces neurological impairment, is a pathological change of CNS injury (49). Reactive astrocytes contribute to beneficial effects via the secretion of neurotrophic substances that protect neurons at early stages (49).

Previous studies have confirmed that MSCs transplantation can increase the expression levels of NeuN (46), MBP (50), and GFAP (51) in brain injuries. Therefore, in order to know the neuroprotective effect of MSCs combined with IronQ after ICH, we further investigated the expression levels of NeuN (the marker of neurons), MBP (the marker of myelin), and GFAP (the marker of astrocytes) through the immunofluorescence and western blot, which are associated with recovery of neurological function (52). We found that the protein expression levels of NeuN, MBP, and GFAP decreased remarkably in mice after ICH. However, an obvious expression increase of NeuN, MBP, and GFAP was seen after giving combined treatment compared with the MSCs transplantation and quercetin gavage. Therefore, our results indicated that the combined treatment might play a synergistic role in increasing the survival of neurons, myelin, and astrocytes, suggesting that combined therapy may ameliorate the hemorrhagic brain injury by promoting survival of neurons, remyelination, and neurotrophic function of astrocytes. Astrocytes are the most abundant cells in the CNS that have multifaceted roles for providing nutrients and recycle neurotransmitters, and fulfilling homeostasis and have been regarded as increasingly important regulators of neuronal functions (49). Our results are consistent with previous studies. After transplantation of MSCs with IronQ in ICH mice, astrocytes underwent astroglial-mesenchymal phenotype switching and became capable of proliferating, and were protected from apoptosis, similarly to previous studies (51, 53). However, some studies have suggested that an excessive proliferation of reactive astrocytes leads to glial scar formation, which is harmful to axon growth and neural network reconstruction (54, 55). It suggests that reactive astrocytes display a double-edged sword function.

As already described, inflammation plays an essential role in ICH and leads to cell swelling and damage, which induces brain edema (56). The moment the blood components are released into the parenchyma, an immediate inflammatory response characterized by the mobilization and activation of inflammatory

cells is triggered (57). Microglia are a major component of the innate immune system, and they respond to acute brain injury after ICH. It has been verified that both innate immunity and inflammation participate in the pathological process of ICH (58, 59).

Mincle is a pattern-recognition receptor, which is mainly expressed on the surface of microglia/macrophages (32, 60–64). Its expression is lower under normal circumstances. During infection and tissue damage, Mincle is upregulated and binds to endogenous antigens, leading to recruitment and activation of syk, and then subsequently activates the NFκB pathway for the activation of innate immunity and host defense, which ultimately generates biologically active inflammatory factors for induction of inflammatory responses (65–68). Previous studies have shown that the Mincle/syk signaling pathway is involved in many innate immune responses, including ischemic stroke, traumatic brain injury, and subarachnoid hemorrhage (30–33, 69). In this study, we found that the MSCs transplantation or quercetin gavage decreased the expression levels of Mincle/Syk signaling pathway-related protein. However, when giving combined treatment, it markedly suppressed the protein expression levels of the Mincle/syk signaling pathway and decreased related proteins associated with inflammation in mice brain tissue following hemorrhage compared with the MSCs transplantation and quercetin gavage. These results suggest that the combined treatment of MSCs with IronQ through the Mincle/Syk signaling pathway mitigates ICH-induced neuroinflammation and improves neural function. Therefore, our results indicated that the combined treatment has synergistic effects on the protein expression levels of Mincle/syk signaling pathway for improving brain damage in mice with ICH. Moreover, blocking the Mincle pathway before CNS injury, brain swelling, and neurological defects were significantly ameliorated (31, 64), suggesting that Mincle-dependent neuroinflammation may be a therapeutic target for ICH treatment.

In summary, we provide evidence for the first time that the Iron-quercetin complex name IronQ is safe for labeling mesenchymal stem cells and tracking the labeled cells in mice with ICH using MRI with T1-weighted techniques. In addition, the first report that combined treatment of MSCs transplantation with IronQ via IronQ-labelled MSCs playing a synergistic role improves ICH-induced brain injury, which is associated with suppression of the Mincle/Syk signaling pathway in mice after ICH. These findings consolidated the protective effects of combined treatment of MSCs with IronQ and supplied positive insights for understanding the underlying molecular mechanisms, which will help us to develop more specific therapeutic drugs; giving us more confidence in the administration and monitoring the stem cells as precise at the target site via magnetic resonance imaging, and helping to treatments for alleviating the neurological outcomes following ICH.

5. Conclusions

This study provided a strategy to enhance the neuroprotective effects of MSCs combined with IronQ complex in collagenase-induced ICH model and demonstrated and the combined treatment plays a synergistic role in ameliorating the consequences of ICH, including neurologic deficits, brain edema, and inflammatory response through the downregulation of the Mincle/syk signaling pathway.

6. List Of Abbreviations

ICH Intracerebral Hemorrhage

MSCs Mesenchymal Stem Cells

MRI Magnetic Resonance Imaging

IronQ Iron-Quercetin Complex

LPS Lipopolysaccharide

BWC Brain Water Content

TCM Traditional Chinese Medicine

PBI Primary Brain Injury

SBI Secondary Brain Injury

CNS Central Nervous System

7. Declarations

Ethics approval and consent to participate

The animal study was reviewed and approved (Approval No. 20211122-040) by the Animal Ethics Research Committee of Southwest Medical University, Luzhou, China.

Consent for publication

Not applicable.

Availability of data and materials

All data generated or analysed during this study are included in this published article [and its supplementary information files].

Competing interests

The authors declare that they have no competing interests.

Funding

This research was funded by Chiang Mai University, National Traditional Chinese Medicine Inheritance and Innovation Team (No: ZYYCXTD-C-202207), the Science and Technology Project of Sichuan Province

(No:2019YFS0543), the Luzhou-Southwest Medical University Science and Technology Strategic Cooperation Project (2021LZXNYD-P04), National Natural Science Foundation of China (No:2021XJYJS02), Brain Disease Innovation Team of the Affiliated Traditional Chinese Medicine Hospital of Southwest Medical University (2022-CXTD-05), Luzhou Science and Technology Project (2020,124), Sichuan Traditional Chinese Medicine Project (2021) No.13, Southwestern Medical University Hospital (2020) No.33, the Project of Southwest Medical University (2021ZKQN125), Sichuan Science and Technology Project (2020YJ0437) and the Project of Sichuan Provincial Administration of Traditional Chinese Medicine (2021MS506).

Authors' Contributions

Conception and design of the study, N.D., L.W. S.Y., H.W.; acquisition and analysis of data, G.Y., J.K., M.M., X.B., Y.X.; drafting a significant portion of the manuscript or figures, G.Y., J.K., M.M.; All authors have read and agreed to the published version of the manuscript.

Acknowledgements

Not applicable

8. References

1. Schrag M, Kirshner H. Management of Intracerebral Hemorrhage: JACC Focus Seminar. J Am Coll Cardiol. 2020;75(15):1819–31.
2. Kirshner H, Schrag M. Management of Intracerebral Hemorrhage: Update and Future Therapies. Curr Neurol Neurosci Rep. 2021;21(10):57.
3. Gross BA, Jankowitz BT, Friedlander RM. Cerebral Intraparenchymal Hemorrhage: A Review. JAMA. 2019;321(13):1295–303.
4. Hanley DF, Thompson RE, Rosenblum M, Yenokyan G, Lane K, McBee N, et al. Efficacy and safety of minimally invasive surgery with thrombolysis in intracerebral haemorrhage evacuation (MISTIE III): a randomised, controlled, open-label, blinded endpoint phase 3 trial. Lancet. 2019;393(10175):1021–32.
5. Feigin VL, Lawes CM, Bennett DA, Barker-Collo SL, Parag V. Worldwide stroke incidence and early case fatality reported in 56 population-based studies: a systematic review. Lancet Neurol. 2009;8(4):355–69.
6. Cordonnier C, Demchuk A, Ziai W, Anderson CS. Intracerebral haemorrhage: current approaches to acute management. Lancet. 2018;392(10154):1257–68.
7. Keep RF, Hua Y, Xi G. Intracerebral haemorrhage: mechanisms of injury and therapeutic targets. Lancet Neurol. 2012;11(8):720–31.
8. Li Z, Li M, Shi SX, Yao N, Cheng X, Guo A, et al. Brain transforms natural killer cells that exacerbate brain edema after intracerebral hemorrhage. J Exp Med. 2020;217(12).

9. Shao Z, Tu S, Shao A. Pathophysiological Mechanisms and Potential Therapeutic Targets in Intracerebral Hemorrhage. Front Pharmacol. 2019;10:1079.
10. Wu X, Luo J, Liu H, Cui W, Guo K, Zhao L, et al. Recombinant Adiponectin Peptide Ameliorates Brain Injury Following Intracerebral Hemorrhage by Suppressing Astrocyte-Derived Inflammation via the Inhibition of Drp1-Mediated Mitochondrial Fission. Transl Stroke Res. 2020;11(5):924–39.
11. Adeoye O, Broderick JP. Advances in the management of intracerebral hemorrhage. Nat Rev Neurol. 2010;6(11):593–601.
12. Mendelow AD, Gregson BA, Rowan EN, Murray GD, Gholkar A, Mitchell PM, et al. Early surgery versus initial conservative treatment in patients with spontaneous supratentorial lobar intracerebral haematomas (STICH II): a randomised trial. Lancet. 2013;382(9890):397–408.
13. Zhou Y, Wang Y, Wang J, Anne Stetler R, Yang QW. Inflammation in intracerebral hemorrhage: from mechanisms to clinical translation. Prog Neurobiol. 2014;115:25–44.
14. Xue M, Yong VW. Neuroinflammation in intracerebral haemorrhage: immunotherapies with potential for translation. Lancet Neurol. 2020;19(12):1023–32.
15. Bao WD, Zhou XT, Zhou LT, Wang F, Yin X, Lu Y, et al. Targeting miR-124/Ferroportin signaling ameliorated neuronal cell death through inhibiting apoptosis and ferroptosis in aged intracerebral hemorrhage murine model. Aging Cell. 2020;19(11):e13235.
16. Gautam J, Xu L, Nirwane A, Nguyen B, Yao Y. Loss of mural cell-derived laminin aggravates hemorrhagic brain injury. J Neuroinflammation. 2020;17(1):103.
17. Tao C, Hu X, Li H, You C. White Matter Injury after Intracerebral Hemorrhage: Pathophysiology and Therapeutic Strategies. Front Hum Neurosci. 2017;11:422.
18. Garcia PY, Roussel M, Bugnicourt JM, Lamy C, Canaple S, Peltier J, et al. Cognitive impairment and dementia after intracerebral hemorrhage: a cross-sectional study of a hospital-based series. J Stroke Cerebrovasc Dis. 2013;22(1):80–6.
19. Oie LR, Madsbu MA, Solheim O, Jakola AS, Giannadakis C, Vorhaug A, et al. Functional outcome and survival following spontaneous intracerebral hemorrhage: A retrospective population-based study. Brain Behav. 2018;8(10):e01113.
20. Li G, Yu F, Lei T, Gao H, Li P, Sun Y, et al. Bone marrow mesenchymal stem cell therapy in ischemic stroke: mechanisms of action and treatment optimization strategies. Neural Regen Res. 2016;11(6):1015–24.
21. Lo Furno D, Mannino G, Giuffrida R. Functional role of mesenchymal stem cells in the treatment of chronic neurodegenerative diseases. J Cell Physiol. 2018;233(5):3982–99.
22. Yang Y, Ye Y, Su X, He J, Bai W, He X. MSCs-Derived Exosomes and Neuroinflammation, Neurogenesis and Therapy of Traumatic Brain Injury. Front Cell Neurosci. 2017;11:55.
23. Tan RZ, Wang C, Deng C, Zhong X, Yan Y, Luo Y, et al. Quercetin protects against cisplatin-induced acute kidney injury by inhibiting Mincle/Syk/NF-kappaB signaling maintained macrophage inflammation. Phytother Res. 2020;34(1):139–52.

24. Zhang Y, Yi B, Ma J, Zhang L, Zhang H, Yang Y, et al. Quercetin promotes neuronal and behavioral recovery by suppressing inflammatory response and apoptosis in a rat model of intracerebral hemorrhage. Neurochem Res. 2015;40(1):195–203.
25. Papan P, Kantapan J, Sangthong P, Meepowpan P, Dechsupa N. Iron (III)-Quercetin Complex: Synthesis, Physicochemical Characterization, and MRI Cell Tracking toward Potential Applications in Regenerative Medicine. Contrast Media Mol Imaging. 2020;2020:8877862.
26. Jiraporn Kantapan SD, Krai Daowtak S, Roytrakul. Padchanee Sangthong, Nathupakorn Dechsupa. Ex vivo expansion of EPCs derived from human peripheral blood mononuclear cells by Iron-Quercetin complex. Biomed Res. 2017;28(6):2730–7.
27. Park JS, Gamboni-Robertson F, He Q, Svetkauskaite D, Kim JY, Strassheim D, et al. High mobility group box 1 protein interacts with multiple Toll-like receptors. Am J Physiol Cell Physiol. 2006;290(3):C917-24.
28. Tang SC, Arumugam TV, Xu X, Cheng A, Mughal MR, Jo DG, et al. Pivotal role for neuronal Toll-like receptors in ischemic brain injury and functional deficits. Proc Natl Acad Sci U S A. 2007;104(34):13798–803.
29. Shichita T, Hasegawa E, Kimura A, Morita R, Sakaguchi R, Takada I, et al. Peroxiredoxin family proteins are key initiators of post-ischemic inflammation in the brain. Nat Med. 2012;18(6):911–7.
30. de Rivero Vaccari JC, Brand FJ 3rd, Berti AF, Alonso OF, Bullock MR, de Rivero Vaccari JP. Mincle signaling in the innate immune response after traumatic brain injury. J Neurotrauma. 2015;32(4):228–36.
31. Suzuki Y, Nakano Y, Mishiro K, Takagi T, Tsuruma K, Nakamura M, et al. Involvement of Mincle and Syk in the changes to innate immunity after ischemic stroke. Sci Rep. 2013;3:3177.
32. He Y, Xu L, Li B, Guo ZN, Hu Q, Guo Z, et al. Macrophage-Inducible C-Type Lectin/Spleen Tyrosine Kinase Signaling Pathway Contributes to Neuroinflammation After Subarachnoid Hemorrhage in Rats. Stroke. 2015;46(8):2277–86.
33. Xie Y, Guo H, Wang L, Xu L, Zhang X, Yu L, et al. Human albumin attenuates excessive innate immunity via inhibition of microglial Mincle/Syk signaling in subarachnoid hemorrhage. Brain Behav Immun. 2017;60:346–60.
34. Zhang X, Liu T, Xu S, Gao P, Dong W, Liu W, et al. A pro-inflammatory mediator USP11 enhances the stability of p53 and inhibits KLF2 in intracerebral hemorrhage. Mol Ther Methods Clin Dev. 2021;21:681–92.
35. Huang S, Xu L, Sun Y, Wu T, Wang K, Li G. An improved protocol for isolation and culture of mesenchymal stem cells from mouse bone marrow. J Orthop Translat. 2015;3(1):26–33.
36. Mazhar M, Yang G, Mao L, Liang P, Tan R, Wang L, et al. Zhilong Huoxue Tongyu Capsules Ameliorate Early Brain Inflammatory Injury Induced by Intracerebral Hemorrhage via Inhibition of Canonical NFsmall ka, Cyrillicbeta Signalling Pathway. Front Pharmacol. 2022;13:850060.
37. Yan J, Xu W, Lenahan C, Huang L, Ocak U, Wen J, et al. Met-RANTES preserves the blood-brain barrier through inhibiting CCR1/SRC/Rac1 pathway after intracerebral hemorrhage in mice. Fluids Barriers

CNS. 2022;19(1):7.
38. Qureshi AI, Mendelow AD, Hanley DF. Intracerebral haemorrhage. Lancet. 2009;373(9675):1632–44.
39. Urday S, Kimberly WT, Beslow LA, Vortmeyer AO, Selim MH, Rosand J, et al. Targeting secondary injury in intracerebral haemorrhage–perihaematomal oedema. Nat Rev Neurol. 2015;11(2):111–22.
40. Wang G, Li Z, Li S, Ren J, Suresh V, Xu D, et al. Minocycline Preserves the Integrity and Permeability of BBB by Altering the Activity of DKK1-Wnt Signaling in ICH Model. Neuroscience. 2019;415:135–46.
41. Gebel JM Jr, Jauch EC, Brott TG, Khoury J, Sauerbeck L, Salisbury S, et al. Natural history of perihematomal edema in patients with hyperacute spontaneous intracerebral hemorrhage. Stroke. 2002;33(11):2631–5.
42. Selim M, Norton C. Perihematomal edema: Implications for intracerebral hemorrhage research and therapeutic advances. J Neurosci Res. 2020;98(1):212–8.
43. Murthy SB, Urday S, Beslow LA, Dawson J, Lees K, Kimberly WT, et al. Rate of perihaematomal oedema expansion is associated with poor clinical outcomes in intracerebral haemorrhage. J Neurol Neurosurg Psychiatry. 2016;87(11):1169–73.
44. Li J, Zhao T, Qiao H, Li Y, Xia M, Wang X, et al. Research progress of natural products for the treatment of ischemic stroke. J Integr Neurosci. 2022;21(1):14.
45. Kim K, Park HW, Moon HE, Kim JW, Bae S, Chang JW, et al. The Effect of Human Umbilical Cord Blood-Derived Mesenchymal Stem Cells in a Collagenase-Induced Intracerebral Hemorrhage Rat Model. Exp Neurobiol. 2015;24(2):146–55.
46. Ding R, Lin C, Wei S, Zhang N, Tang L, Lin Y, et al. Therapeutic Benefits of Mesenchymal Stromal Cells in a Rat Model of Hemoglobin-Induced Hypertensive Intracerebral Hemorrhage. Mol Cells. 2017;40(2):133–42.
47. Wasserman JK, Schlichter LC. White matter injury in young and aged rats after intracerebral hemorrhage. Exp Neurol. 2008;214(2):266–75.
48. Tao C, Zhang R, Hu X, Song L, Wang C, Gao F, et al. A Novel Brainstem Hemorrhage Model by Autologous Blood Infusion in Rat: White Matter Injury, Magnetic Resonance Imaging, and Neurobehavioral Features. J Stroke Cerebrovasc Dis. 2016;25(5):1102–9.
49. Pekny M, Pekna M. Astrocyte reactivity and reactive astrogliosis: costs and benefits. Physiol Rev. 2014;94(4):1077–98.
50. Tapia-Bustos A, Lespay-Rebolledo C, Vio V, Perez-Lobos R, Casanova-Ortiz E, Ezquer F, et al. Neonatal Mesenchymal Stem Cell Treatment Improves Myelination Impaired by Global Perinatal Asphyxia in Rats. Int J Mol Sci. 2021;22(6).
51. Chen X, Liang H, Xi Z, Yang Y, Shan H, Wang B, et al. BM-MSC Transplantation Alleviates Intracerebral Hemorrhage-Induced Brain Injury, Promotes Astrocytes Vimentin Expression, and Enhances Astrocytes Antioxidation via the Cx43/Nrf2/HO-1 Axis. Front Cell Dev Biol. 2020;8:302.
52. Lan X, Han X, Li Q, Yang QW, Wang J. Modulators of microglial activation and polarization after intracerebral haemorrhage. Nat Rev Neurol. 2017;13(7):420–33.

53. Chen X, Xu CX, Liang H, Xi Z, Pan J, Yang Y, et al. Bone marrow mesenchymal stem cells transplantation alleviates brain injury after intracerebral hemorrhage in mice through the Hippo signaling pathway. Aging. 2020;12(7):6306–23.
54. Zhu YM, Gao X, Ni Y, Li W, Kent TA, Qiao SG, et al. Sevoflurane postconditioning attenuates reactive astrogliosis and glial scar formation after ischemia-reperfusion brain injury. Neuroscience. 2017;356:125–41.
55. Pekny M, Pekna M, Messing A, Steinhauser C, Lee JM, Parpura V, et al. Astrocytes: a central element in neurological diseases. Acta Neuropathol. 2016;131(3):323–45.
56. Tschoe C, Bushnell CD, Duncan PW, Alexander-Miller MA, Wolfe SQ. Neuroinflammation after Intracerebral Hemorrhage and Potential Therapeutic Targets. J Stroke. 2020;22(1):29–46.
57. Xiao L, Zheng H, Li J, Wang Q, Sun H. Neuroinflammation Mediated by NLRP3 Inflammasome After Intracerebral Hemorrhage and Potential Therapeutic Targets. Mol Neurobiol. 2020;57(12):5130–49.
58. Fang H, Wang PF, Zhou Y, Wang YC, Yang QW. Toll-like receptor 4 signaling in intracerebral hemorrhage-induced inflammation and injury. J Neuroinflammation. 2013;10:27.
59. Guo H, Zhang Y, Hu Z, Wang L, Du H. Screening and identification of biomarkers associated with the immune infiltration of intracerebral hemorrhage. J Clin Lab Anal. 2022;36(5):e24361.
60. Flornes LM, Bryceson YT, Spurkland A, Lorentzen JC, Dissen E, Fossum S. Identification of lectin-like receptors expressed by antigen presenting cells and neutrophils and their mapping to a novel gene complex. Immunogenetics. 2004;56(7):506–17.
61. McKimmie CS, Roy D, Forster T, Fazakerley JK. Innate immune response gene expression profiles of N9 microglia are pathogen-type specific. J Neuroimmunol. 2006;175(1–2):128–41.
62. Ribbing C, Engblom C, Lappalainen J, Lindstedt K, Kovanen PT, Karlsson MA, et al. Mast cells generated from patients with atopic eczema have enhanced levels of granule mediators and an impaired Dectin-1 expression. Allergy. 2011;66(1):110–9.
63. Kawata K, Illarionov P, Yang GX, Kenny TP, Zhang W, Tsuda M, et al. Mincle and human B cell function. J Autoimmun. 2012;39(4):315–22.
64. Yamasaki S, Ishikawa E, Sakuma M, Hara H, Ogata K, Saito T. Mincle is an ITAM-coupled activating receptor that senses damaged cells. Nat Immunol. 2008;9(10):1179–88.
65. Takizawa T, Tada T, Kitazawa K, Tanaka Y, Hongo K, Kameko M, et al. Inflammatory cytokine cascade released by leukocytes in cerebrospinal fluid after subarachnoid hemorrhage. Neurol Res. 2001;23(7):724–30.
66. Strasser D, Neumann K, Bergmann H, Marakalala MJ, Guler R, Rojowska A, et al. Syk kinase-coupled C-type lectin receptors engage protein kinase C-delta to elicit Card9 adaptor-mediated innate immunity. Immunity. 2012;36(1):32–42.
67. Yasukawa S, Miyazaki Y, Yoshii C, Nakaya M, Ozaki N, Toda S, et al. An ITAM-Syk-CARD9 signalling axis triggers contact hypersensitivity by stimulating IL-1 production in dendritic cells. Nat Commun. 2014;5:3755.

68. He X, Huang Y, Liu Y, Zhang X, Yue P, Ma X, et al. BAY613606 attenuates neuroinflammation and neurofunctional damage by inhibiting microglial Mincle/Syk signaling response after traumatic brain injury. Int J Mol Med. 2022;49(1).
69. Arumugam TV, Manzanero S, Furtado M, Biggins PJ, Hsieh YH, Gelderblom M, et al. An atypical role for the myeloid receptor Mincle in central nervous system injury. J Cereb Blood Flow Metab. 2017;37(6):2098–111.

Figures

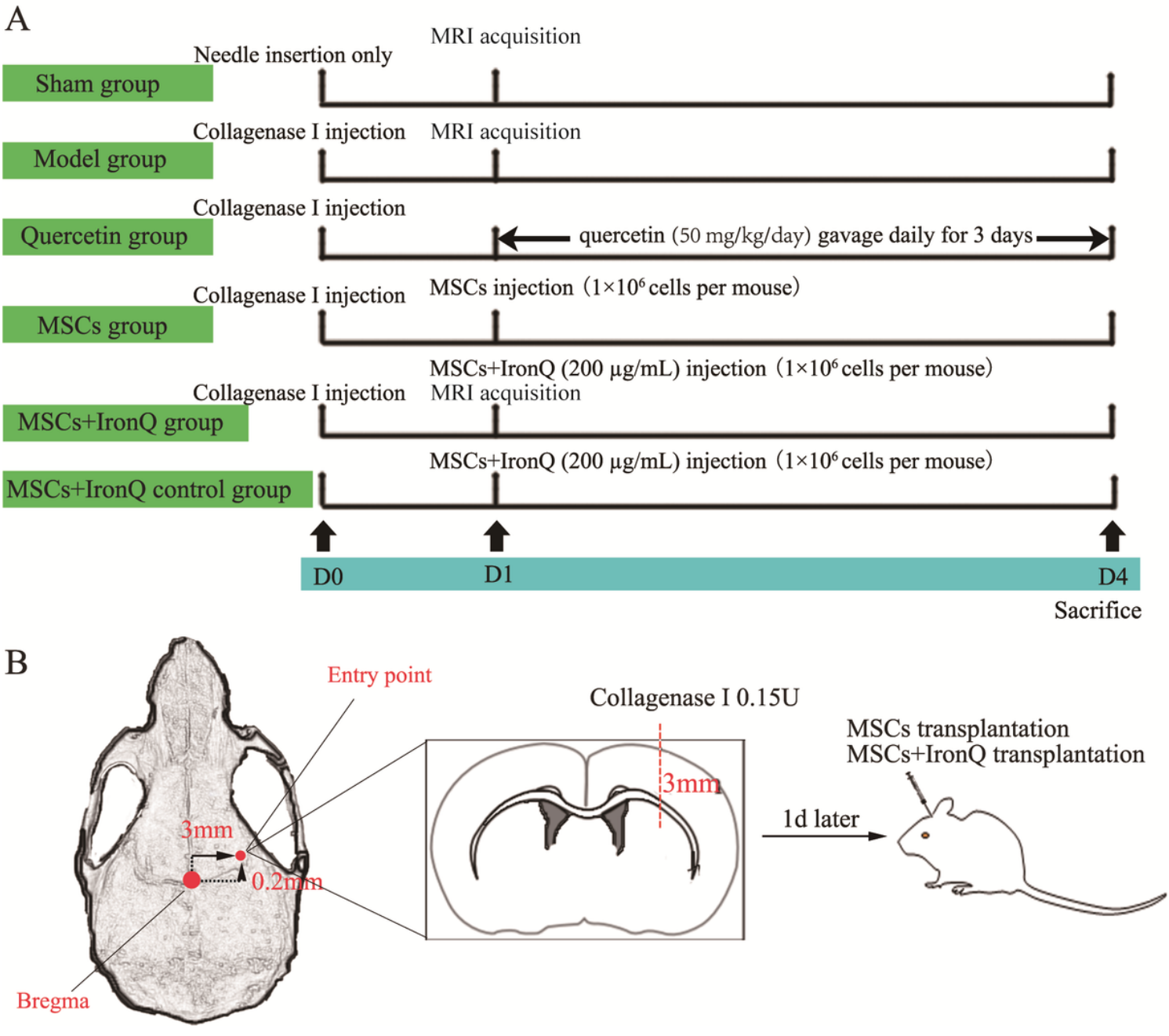

Figure 1

Conceptual illustrations of the experimental protocols. (A) Grouping and treatment strategies for experimental mice and a brief timeline of the experimental procedures. (B) Schematic diagrams of the mouse ICH model along with MSC and MSCs+IronQ transplantation.

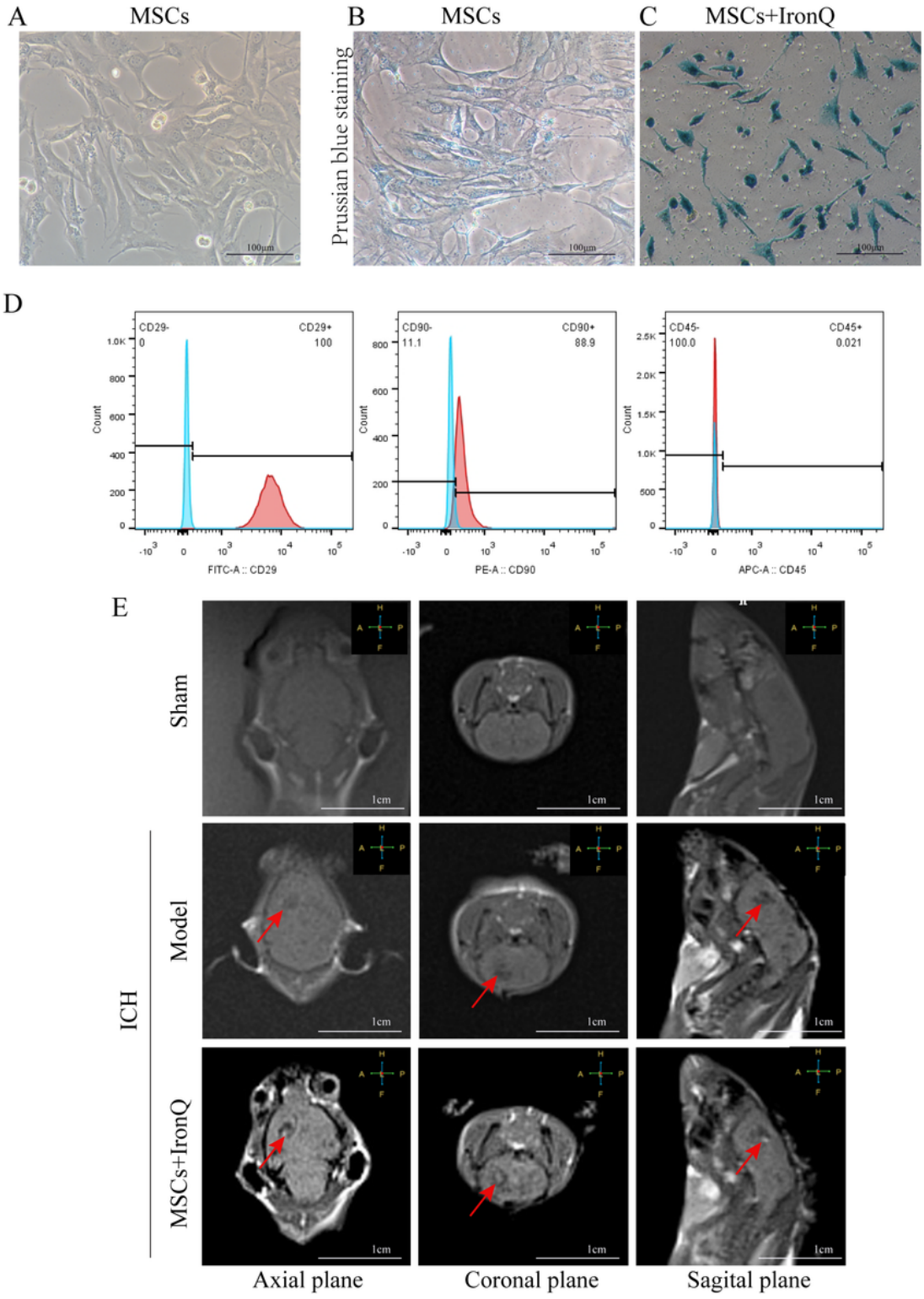

Figure 2

The images of MSCs and the IronQ-labeled MSCs from an inverted phase-contrast microscope and 3.0T MRI. **(A)** MSCs at passage 3-6 grew in cluster shape. Scale bar = 100μm. **(B-C)** The images of MSCs incubated without (**B**) and with (**C**) IronQ for 24 hours checked by Prussian blue staining. Scale bar = 100 μm. **(D)** The identification results of MSCs by flow cytometry. **(E)** T1W images of mice brains in the coronal plane, axial plane, and sagittal plane of the sham, ICH model, and MSCs+IronQ treatment groups. Arrow indicates hemorrhage (dark) area and IronQ-labeled MSCs (a white spot) in the hemorrhage (dark) area in the brain tissue of ICH mice. Scale bar =1cm.

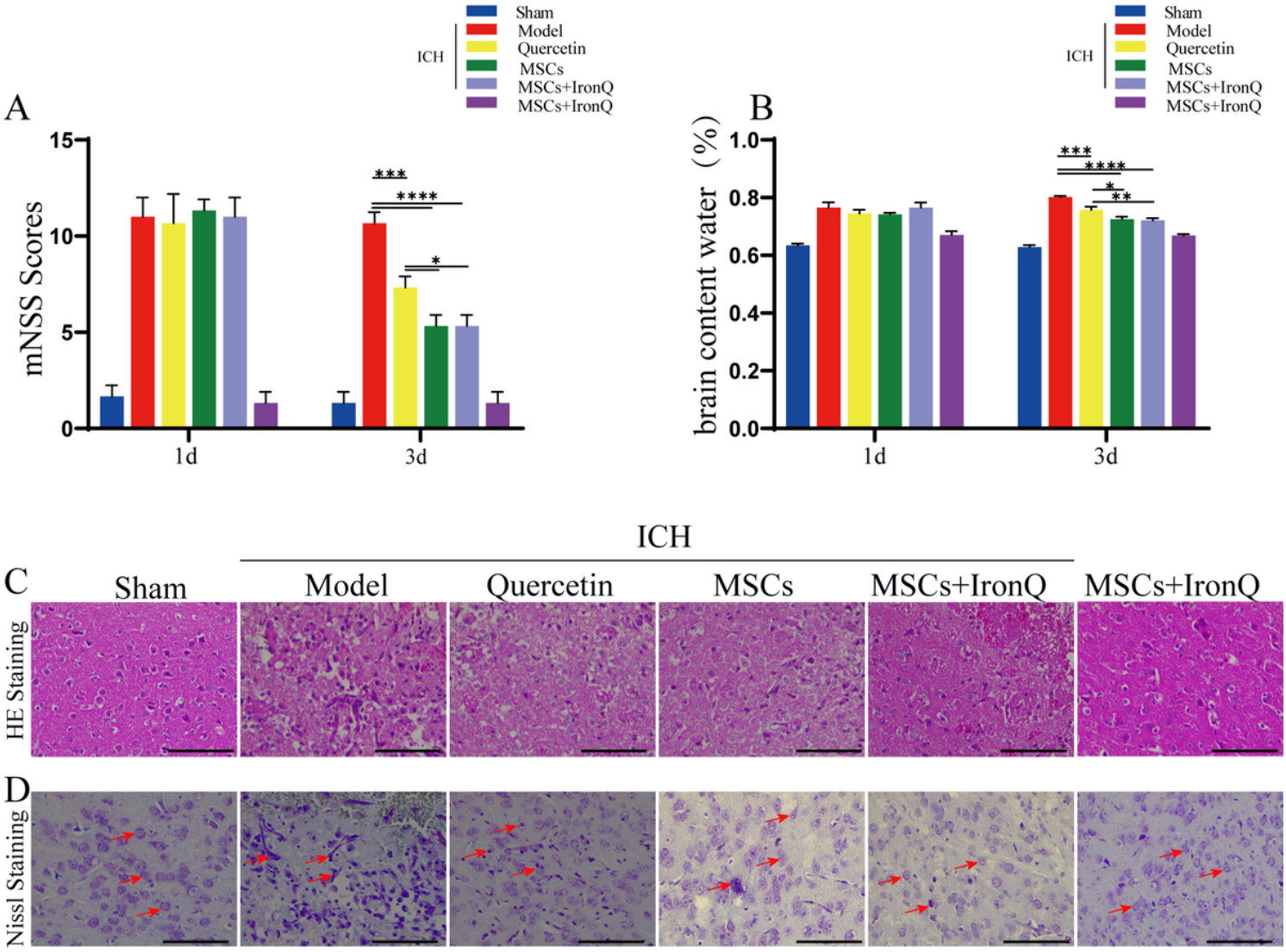

Figure 3

MSCs+IronQ transplantation attenuated the neurological deficits and protected the brain parenchyma and neurons in mice ICH

(A) The results of mNSS displayed the points of mice in different groups in 1d and 3d (n = 5 per group; * $P < 0.05$, *** $P < 0.001$, and **** $P < 0.0001$). **(B)** BWC of brain samples in different groups (n= 5per group; * $P < 0.05$, ** $P < 0.01$, *** $P < 0.001$, and **** $P < 0.0001$). **(C)** HE staining of brain samples was performed

in mice in different groups. Scale bar = 100 μm. **(D)** Nissal staining of brain samples was performed in different groups. Scale bar =100 μm.

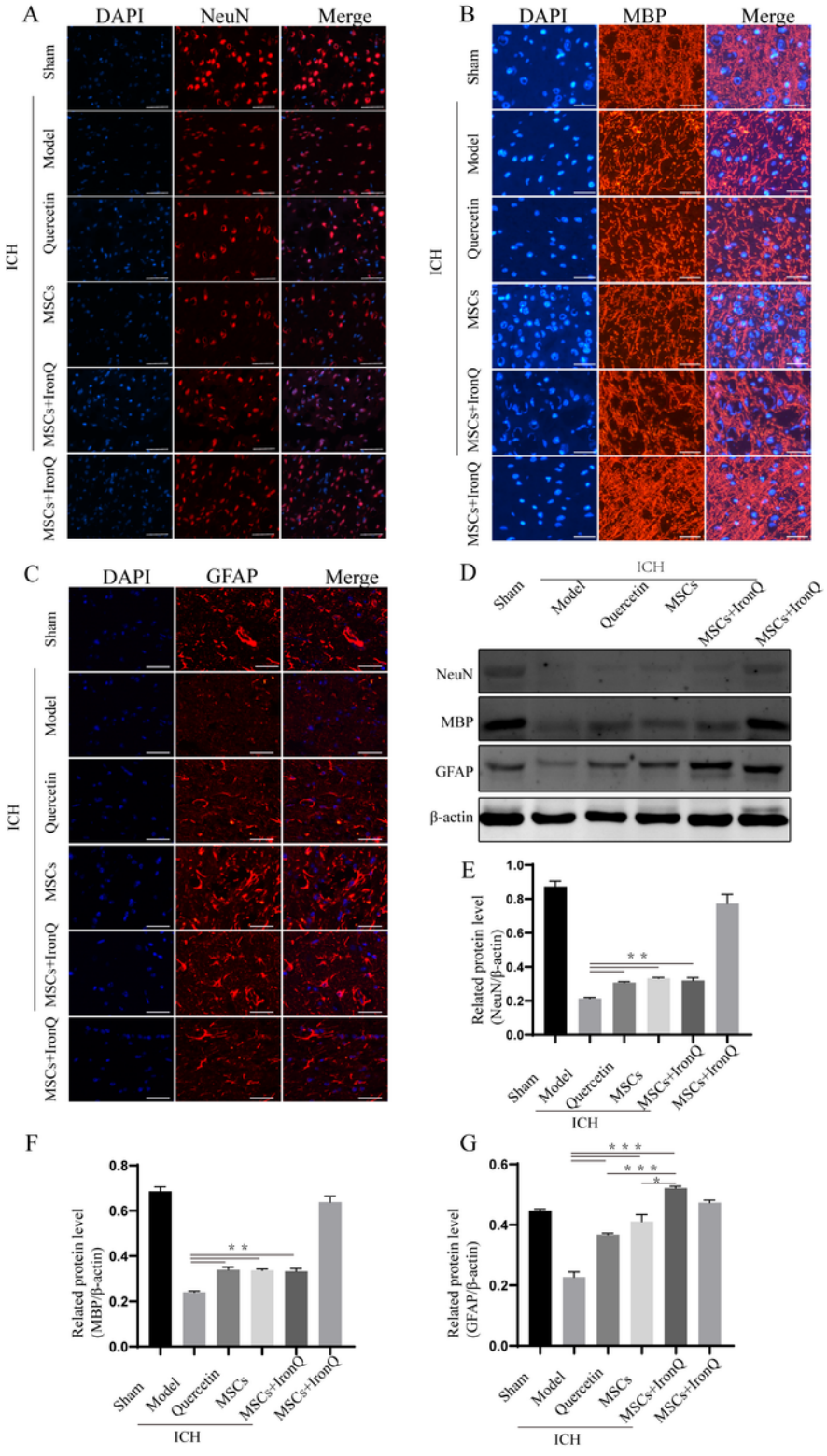

Figure 4

MSCs and IronQ Combined treatment enhanced the expression level of NeuN, MBP, and GFAP in mice with ICH (**A-C**) The results of immunofluorescence displayed the protein expression levels of NeuN, MBP,

and GFAP in mice after ICH (n = 5 per group). (**D-G**) Western blot results and analysis for the protein expression levels of NeuN, MBP, and GFAP (n = 5 per group; $^{**}P < 0.05$, $^{**}P < 0.01$, $^{***}P < 0.001$).

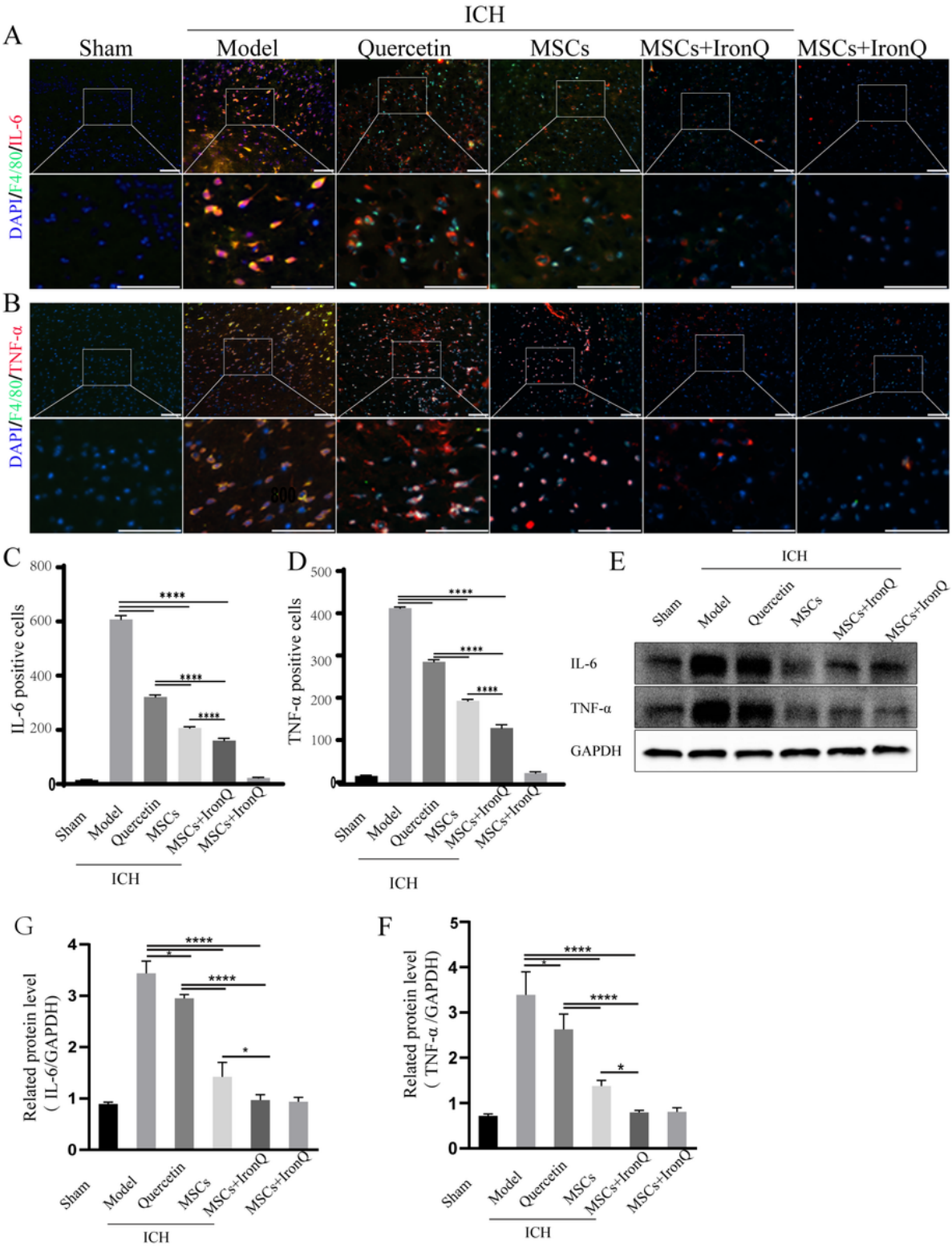

Figure 5

MSCs and IronQ Combined treatment decreased the inflammatory reponse in mice with ICH. (**A,B**) The results of double immunofluorescence displayed co-localization for F480 co-expressing with IL-6 and

TNF-α in mice after ICH. (**C,D**) showed the statistical graph of positive cells of IL-6 and TNF-α (n= 5 per group; ***$P < 0.001$, and ****$P < 0.0001$). (**E,F**) Westernblot results displayed that combined treatment decreased the poritein levels of IL-6 and TNFa (n = 5per group; *$P < 0.05$, and ****$P < 0.0001$).

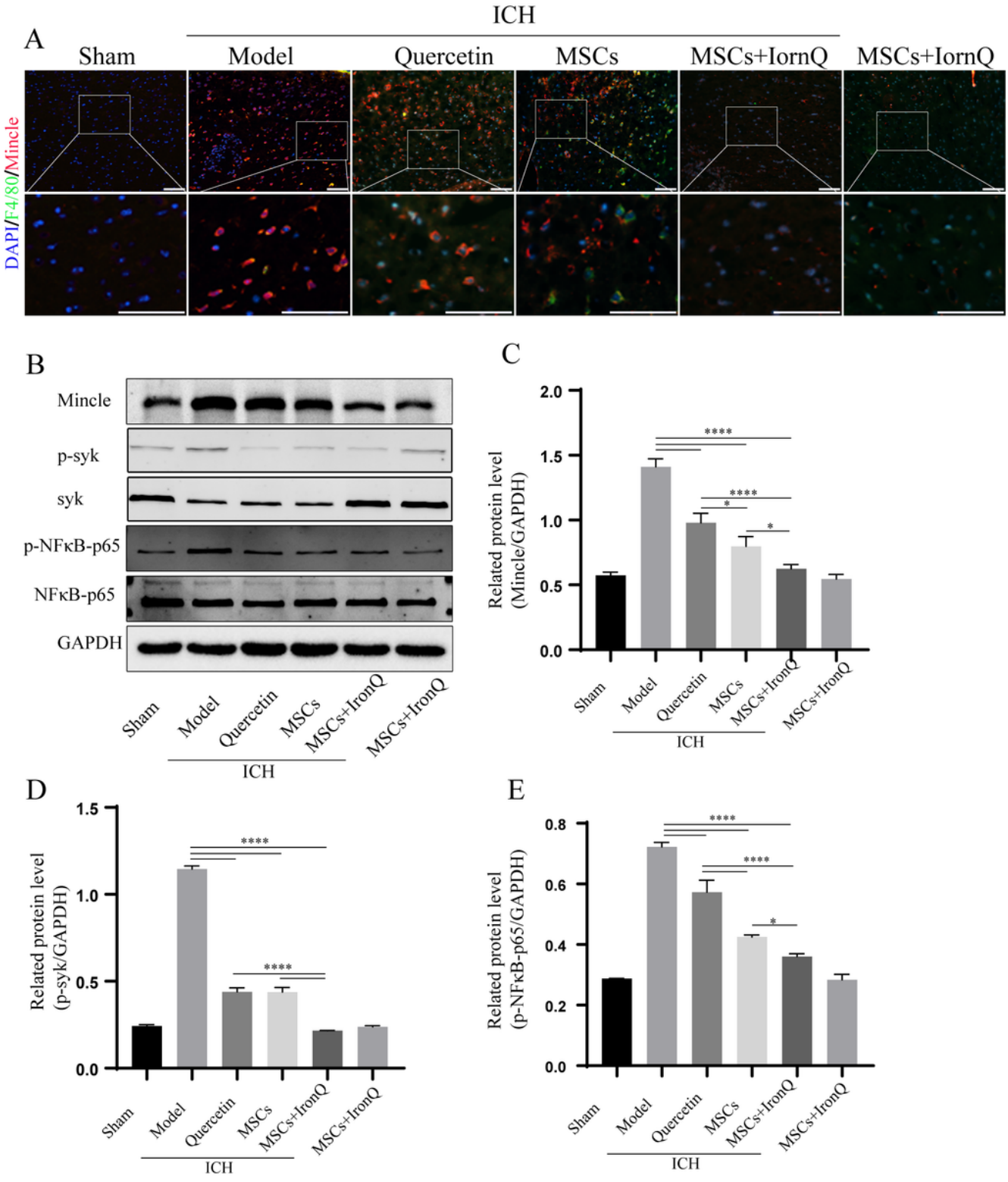

Figure 6

MSCs and IronQ Combined treatment regulated the Mincle/syk signaling pathway to improve of ICH outcomes. (**A**) The results of double immunofluorescence displayed co-expression level of Mincle and F4/80 in different groups (n = 5 per group). (**B-E**) Western blot results and analysis showed the protein expression levels of Mincle, p-syk, p-NFκB-p65 in mice with ICH in different groups (n = 5 per group; **P* < 0.05, and *****P* < 0.0001).

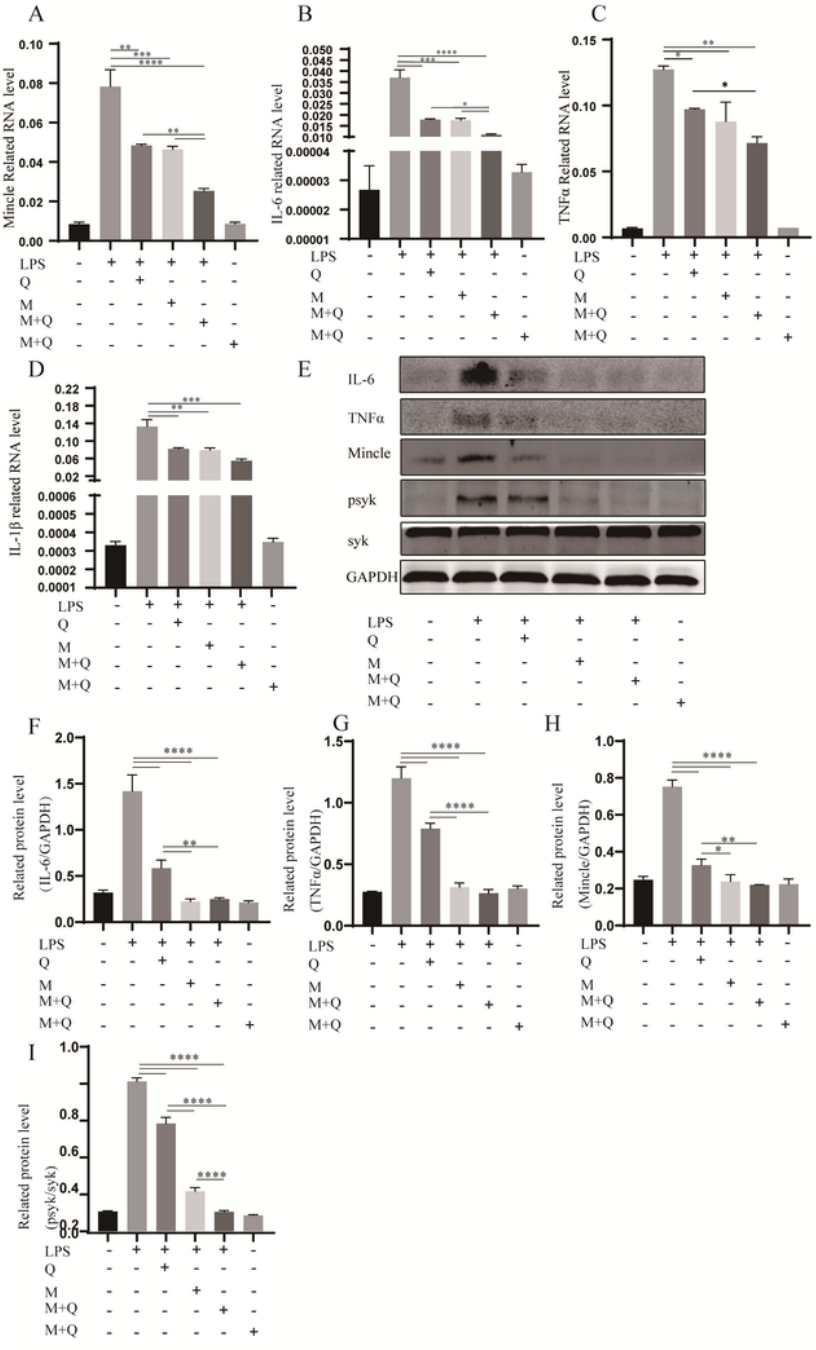

Figure 7

The results of RT-qPCR and western blot revealed that the conditional medium of MSCs with IronQ treatment reduced mRNA and protein expression levels of Mincle and its related inflammatory factors. Graphs showing relative expression levels of mRNA **(A)** Mincle, **(B)** IL-6, **(C)** TNF-α, and **(D)** IL-1β; in different cells groups after 6h (n = 3 per group; **P* < 0.05, ***P* < 0.01, ****P* < 0.001, and *****P* < 0.0001). (**E-I**) showed that the results and analyses of western blot about the conditional medium of MSCs with IronQ downregulating the protein expression levels of IL-6, TNF-α, Mincle, and p-syk in LPS-induced BV2 cell line. **(E)** Representative immunoblot showing the protein expression levels of IL-6,TNF-α, Mincle, syk, p-syk, and GAPDH; **(F)** the quantitative densitometric ratio of IL-6, **(G)** TNF-α, **(H)** Mincle and **(I)** p-syk relative to GAPDH (n = 3 per group; **P* < 0.05, ***P* < 0.01, and *****P* < 0.0001). The conditional medium of MSCs with IronQ treatment reduced the protein expression levels of Mincle and its downstream protein syk in the LPS-induced BV2 cell line after 24h.

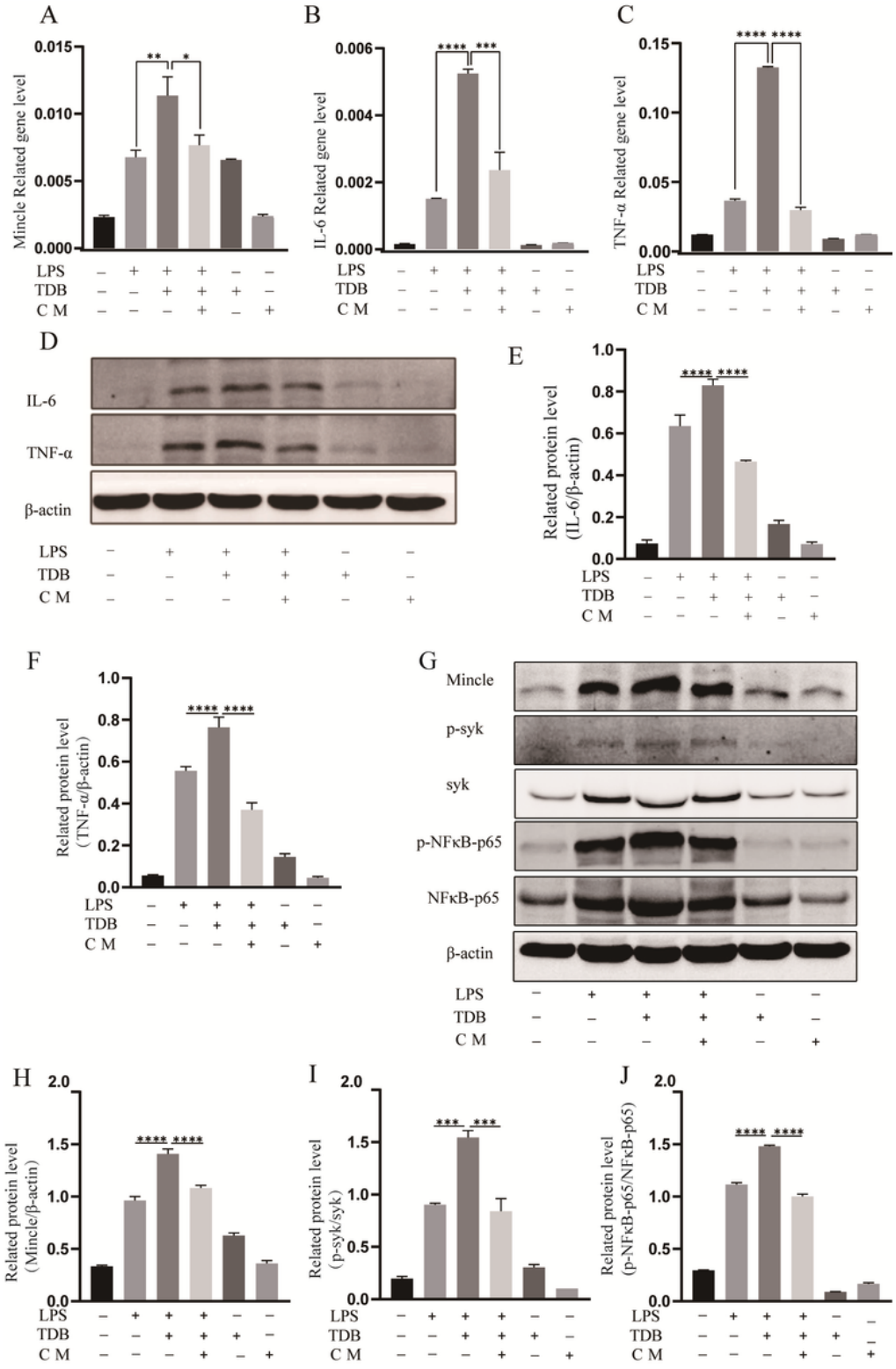

Figure 8

The results and analyses of RT-qPCR and western blot revealed the conditional medium of MSCs with IronQ treatment reduced inflammatory response by regulating the Mincle/syk signaling pathway. Graphs showing relative expression levels of mRNA **(A)** Mincle, **(B)** IL-6, and **(C)** TNF-α; in different cell groups after 6 h (n = 3 per group; *P < 0.05, **P < 0.01, ***P < 0.001, and ****P < 0.0001). Western blot demonstrated conditional medium of MSCs with IronQ downregulated the protein expression of IL-6, TNF-

α, Mincle, p-syk, p-NFκB-p65 in the LPS-induced BV2 cell line (**Figure 7E-I**). **(E)** Representative immunoblot showing the effect of conditional medium on protein expression of IL-6, TNF-α, Mincle, syk, p-syk, p-NFκB-p65, p-NFκB-p65, and GAPDH; **(F)** the quantitative densitometric ratio of IL-6, **(G)** TNF-α, **(H)** Mincle and **(I)** p-syk (J) p-NFκB-p65 relative to GAPDH (n = 3 per group; ****$P < 0.0001$). The conditional medium of MSCs with IronQ treatment reduced the protein expression of Mincle and its downstream, p-syk and p-NFκB-p65 after 24h.